Label-free, live optical imaging of reprogrammed bipolar disorder patient-derived cells reveals a functional correlate of lithium responsiveness

OPEN

Citation: Transl Psychiatry (2014) 4, e428; doi:10.1038/tp.2014.72

www.nature.com/tp

ORIGINAL ARTICLE

Label-free, live optical imaging of reprogrammed bipolar disorder patient-derived cells reveals a functional correlate of lithium responsiveness

JL Wang[1,2,3], SM Shamah[4], AX Sun[5], ID Waldman[6], SJ Haggarty[1,2,3,7] and RH Perlis[1,2,3]

Development of novel treatments and diagnostic tools for psychiatric illness has been hindered by the absence of cellular models of disease. With the advent of cellular reprogramming, it may be possible to recapitulate the disease biology of psychiatric disorders using patient skin cells transdifferentiated to neurons. However, efficiently identifying and characterizing relevant neuronal phenotypes in the absence of well-defined pathophysiology remains a challenge. In this study, we collected fibroblast samples from patients with bipolar 1 disorder, characterized by their lithium response ($n = 12$), and healthy control subjects ($n = 6$). We identified a cellular phenotype in reprogrammed neurons using a label-free imaging assay based on a nanostructured photonic crystal biosensor and found that an optical measure of cell adhesion was associated with clinical response to lithium treatment. This cellular phenotype may represent a useful biomarker to evaluate drug response and screen for novel therapeutics.

Translational Psychiatry (2014) **4,** e428; doi:10.1038/tp.2014.72; published online 26 August 2014

INTRODUCTION

Bipolar disorder (BD) is a debilitating psychiatric condition characterized by periods of elevated or irritable mood and depression.[1,2] Since its serendipitous discovery over 50 years ago, lithium remains the gold-standard treatment for long-term management of BD.[3] However, lithium only benefits a subset of individuals with this illness.[4]

There is thus a pressing need for better therapeutics, as well as diagnostic tools which might predict patient drug response. The challenge has been identifying a distinct cellular pathophysiology associated with the disorder. Investigators have generally been limited to the study of peripheral blood cells or postmortem brain samples, each of which presents limitations, both in determining relevance to the neurobiology of BD and in deriving cellular models which scale for screening applications and diagnostic development.

Recent developments in reprogrammed adult human cells make it possible to derive neuronal cells directly from more accessible patient tissues, either through an induced pluripotent stem cell intermediate[5–7] or via direct transdifferentiation of human fibroblasts to neurons.[8–10] These reprogrammed cellular models have been demonstrated to recapitulate disease pathology observed in primary human brain cells for neurodegenerative disorders such as Alzheimer's disease and Parkinson's disease.[11] Efficiently identifying and characterizing relevant neuronal phenotypes in the absence of well-defined pathophysiology remains a challenge. Here, we hypothesized that lithium response in BD patients would have a measurable cellular correlate in patient fibroblast lines directly transdifferentiated to neurons using a high-throughput, label-free imaging platform.

In this label-free cellular assay, the signal generated is a measure of adhesion of the cell to the imaged surface, mediated by cell surface integrins and extracellular matrix components coated on the surface of biosensors. Once adhered to the biosensors, cells respond to a wide variety of stimuli that result in the modulation of cell adhesion mediated by changes in the activation state of integrins through a process referred to as 'inside-out signaling'.[12] These changes can be measured and quantified with high sensitivity and serve the basis of functional cell-based assays for identifying compounds that can modulate specific ligand–receptor signaling pathways.[13,14] The BIND Scanner used in our experiments has sufficiently high spatial and temporal resolution that single cell morphologies can be segmented and a number of cellular phenotypes quantified, including cell migration, membrane ruffling, mitotic events, apoptosis, proliferation and immune cell activation.[14] This makes the platform particularly advantageous for characterizing disease-associated cellular phenotypes, which may be applied for high-throughput screening or diagnostic efforts. In our study, we examined changes in cell count, cell fraction, cell perimeter and peak wavelength value (PWV), which is a measure of the attachment of the cells to the surface. We found that changes in PWV were associated with patient lithium response in fibroblasts transdifferentiated to neuronal-like cells.

MATERIALS AND METHODS

Patient sample collection

Skin samples from a convenience sample of patients with bipolar 1 disorder and a history of lithium treatment ($n = 12$) and matched screened

[1]Department of Psychiatry, Center for Experimental Drugs and Diagnostics, Massachusetts General Hospital, Boston, MA, USA; [2]Center for Human Genetics Research, Massachusetts General Hospital, Boston, MA, USA; [3]Stanley Center for Psychiatric Research, Broad Institute of MIT & Harvard, Cambridge, MA, USA; [4]X-Body Biosciences, Waltham, MA, USA; [5]Howard Hughes Medical Institute, Stanford University School of Medicine, Stanford, CA, USA; [6]Department of Psychology, Emory University, Atlanta, GA, USA and [7]Chemical Neurobiology Laboratory, Department of Neurology, Massachusetts General Hospital, Harvard Medical School, Boston, MA, USA. Correspondence: Dr RH Perlis, Department of Psychiatry, Center for Experimental Drugs and Diagnostics and Center for Human Genetics Research, Simches Research Building, Massachusetts General Hospital, 185 Cambridge Street, 6th Floor, Boston, MA 02114, USA.
E-mail: rperlis@mgh.harvard.edu
Received 8 July 2014; accepted 14 July 2014

healthy control subjects ($n = 6$) were collected after obtaining written informed consent as part of a protocol approved by the Partners Institutional Review Board. All subjects were evaluated using the structured clinical interview for DSM-IV (SCID-I) conducted by an experienced psychiatrist. Lifetime lithium response was defined by clinical interview and review of all available records using the Alda scale for long-term treatment response in research subjects with bipolar disorder,[15] which assigns a 0–10 score ('Criterion A') for clinical improvement during lithium treatment compared with time not treated with lithium, in terms of episode frequency, severity and duration. On this scale, 10 indicates full and sustained remission with lithium treatment, whereas 0 indicates no change or clinical worsening. This scale, although retrospective, has been shown to be a reliable and valid summary measurement of lithium responsiveness. As the utility and weighting of the B criteria, relating to features such as compliance, is less clear,[16] we selected extreme cases based upon A criteria, excluding individuals who were nonadherent with lithium based upon the relevant B criterion. We grouped BD patients into a lithium responsive group if the Alda score was 7–10, and lithium nonresponsive if the Alda score was 1–4.

Clinical procedures

After informed consent was obtained and clinical interview was completed to confirm eligibility, a dermal biopsy was obtained by a physician investigator. Following subcutaneous injection of lidocaine 1%, the physician used a standard 3.0 or 4.0 mm punch tool to obtain a sample from the medial surface of the nondominant forearm. Fibroblasts were then expanded using standard tissue culture technique.

Lentivirus production

High-titer lentiviral stocks were generated using 293T/17 cells (ATCC, Manassas, VA, USA). Cells were plated on poly-L-Lysine (Sigma, St. Louis, MO, USA) coated tissue culture vessels and grown to 95% confluence in D10 medium containing Dulbecco's Modified Eagle Medium (Invitrogen, Carlsbad, CA, USA) with 10% fetal bovine serum (Gemini Bio-Products, West Sacramento, CA, USA) and 1% Pen-Strep (Invitrogen), then transfected with lentiviral packaging plasmids pCMV2dR8.2 (Addgene plasmid 8455, Cambridge, MA, USA)[17] and pMD2.G (Addgene plasmid 12259) and one of the lentivectors containing transgenes for miR-9/9*-124, *NEUROD2*, *ASCL1* or *MYT1L* using Lipofectamine 2000 (Invitrogen) in Optimem (Invitrogen). After 4–6 h, the medium was changed back to D10 medium, collected after 48 h and ultracentrifuged at 19 500 r.p.m. for 2 h to make high-titer lentiviral stocks.

Induced neuronal-like cells

Fibroblasts were transduced with lentiviruses containing transgenes for miR-9/9*-124, *NEUROD2*, *ASCL1* and *MYT1L* as previously described.[9] Fibroblasts were plated at a density of 10–15 k cm^{-2} in fibroblast medium (Dulbecco's Modified Eagle Medium; Invitrogen) containing 10% fetal bovine serum (FBS; Gemini Bio-Products), nonessential amino acids, glutamate and penicillin/streptomycin (Invitrogen) on plates coated with 0.1% gelatin (Millipore, Billerica, MA, USA). Fibroblast medium contained DMEM (Invitrogen) with 10% FBS (Gemini Bio-Products), 1% Pen-Strep (Invitrogen, Grand Island, NY, USA), 1% non-essential amino acids (Invitrogen) and 1% 200 mM L-glutamine (Invitrogen). Infection with the four lentiviruses occurred 24 h after plating using 8 μg ml^{-1} polybrene (Sigma) with plates centrifuged at 1000 g for 20 min to enhance the lentivirus infection efficiency. The next day, medium was changed to fibroblast medium containing 1 mM valproic acid (Sigma), and 3 days later, the medium was changed to Neuronal Medium (ScienCell, Carlsbad, CA, USA) containing 1 mM valproic acid along with selection antibiotics Geneticin, Blasticidin and Puromycin (all Invitrogen). Selection antibiotics were removed after 6–7 days, and the cells were maintained in Neuronal Medium (ScienCell) with 1 mM valproic acid for 1–3 days until passaging with Accutase (Sigma) onto a 384-well BIND biosensor.

BIND imaging

BIND biosensors used for induced neuronal-like cell (iNLC) imaging were coated with 20 μg ml^{-1} poly-ornithine (Sigma) and 20 μg ml^{-1} laminin (Sigma) and biosensors used for fibroblast imaging were coated with 2.5 μg ml^{-1} fibronectin (BD Biosciences, San Jose, CA, USA). iNLCs were seeded at 1000 cells per well, and human fibroblasts were seeded at 200 cells per well. Biosensors were blocked with 1% bovine serum albumin (Sigma) in Dulbecco's phosphate-buffered saline (dPBS, Invitrogen) before plating cells to minimize background. After seeding cells, the biosensor was briefly centrifuged at 1000 r.p.m. for 10 s to ensure that the cells were contacting the biosensor. The biosensor was equilibrated at 37 °C for 15–30 min before imaging. Time-lapse BIND images were collected using BIND Scan software.

Immunocytochemistry

At the same time point and density that iNLCs were plated on BIND biosensors, they were plated on poly-ornithine/laminin coated 384-well plates for immunocytochemistry. Corresponding fibroblast lines were seeded at 1000 cells per well in 384 well plates. One day later, cells were fixed in 4% formaldehyde (Tousimis) in dPBS for 30 min at 25 °C, rinsed three times in PBS, and then incubated overnight at 4 °C with primary antibodies against Fibroblast (1:10, Miltenyi Biotec, Bergisch Gladbach, Germany), *FSP1/S100A4* (1:750, Millipore), *VIM* (1:50, Abcam, Cambridge, UK), *SOX2* (1:200, Abcam), *NES* (1:500, Millipore), *MAP2* (1:5000, EnCor Biotechnology CPCA-MAP2, Gainesville, FL, USA), *TUBB3* (1:5000, Sigma T8660) and *SYN1* (1:200, Cell Signaling, Danvers, MA, USA) in a blocking solution containing 0.1% Triton, 5% normal goat serum (Invitrogen) and 0.1% gelatin (Sigma) in dPBS. Cells were rinsed five times with dPBS, then incubated for 1 h at 25 °C with an Alexa Fluor 488 secondary antibody corresponding to the primary (1:500, Invitrogen A-11039, A-11034 and A-11029) in the same blocking solution containing NucBlue Hoechst 33342 (Life Technologies, Grand Island, NY, USA) to label cellular nuclei. Cells were rinsed three times in dPBS, and images were acquired using an INCell 6000 (GE Healthcare, Piscataway, NJ, USA). Images were rescaled and pseudocolored using Fiji for display purposes with the same range used for each antibody across both cell types.

Data analysis

BIND Scan data was segmented and cellular metrics quantified using BIND View software. Background leveling was implemented with a 17-pixel structural morphological parameter. Segmented objects were classified as cells if they had a PWV minimum of 0.2–0.35 nm and a maximum of 5 nm above background and had an area greater than 10 pixels. A local background area around each segmented cell was calculated from a 2-pixel radius located 3 pixels outside the boundary of the cell. The average PWV from this local background area was subtracted from the average PWV inside the boundary of the cell to calculate the cellular PWV metric. Cell count, cell fraction and cell perimeter were computed from the mask of the segmented cells. These metrics were exported for each image in the time-lapse series and comprised the time series data in Figure 1b. Delta metrics were calculated as:

$$\Delta\text{metric} = \frac{\text{metric}_{1.5\text{h}} - \text{metric}_{\text{baseline}}}{\text{metric}_{\text{baseline}}}$$

GLMs utilized the 'glm' command in Stata 13 (StataCorp, College Station, TX, USA) with default settings for family (Gaussian) and link function (identity), and observations clustered within patients. Including within-plate clustering as well, rather than covarying for plate, did not yield meaningfully different results.

RESULTS

Generation of iNLCs

Skin samples from a clinically phenotyped cohort of patients with bipolar 1 disorder and a history of lithium treatment ($n = 12$) and matched screened healthy control subjects ($n = 6$) were expanded into fibroblast lines and subsequently transformed using recombinant lentiviruses carrying transgenes for miR-9/9*-124, *NEUROD2*, *ASCL1* and *MYT1L*.[9] This transformation results in iNLCs, directly transdifferentiated from the starting fibroblast population. The full duration of time to generate 'mature' neuronal-like cells that express synaptic markers and fire action potentials as described by Yoo *et al*.[9] is 4–5 weeks. However, due to reduced viability we observed over this prolonged time period of differentiation, and the goal of a more rapid screening process, we elected to measure cellular activity at an earlier time point in the transdifferentiation process to facilitate generating reproducible measurements over larger numbers of iNLCs. This period,

13–14 days posttransduction, occurs after antibiotic selection for cells expressing the transgenes, but before the large amount of cellular attrition. Figure 2a shows the timeline of the neural induction.

At this time point, cells are undergoing large morphological changes reminiscent of axonogenesis and dendritogenesis in rodent neurons. We performed immunocytochemistry to characterize the iNLCs along with the source patient fibroblast line. We selected a panel of antibodies to label fibroblasts (anti-Fibroblast), fibroblasts and neural stem cells (*S100A4, VIM)*, neural stem cells only (*NES, SOX2)* and neurons (*MAP2, TUBB3, SYN1*). Images for a representative control line are shown in Supplementary Figure 1. Anti-Fibroblast labeled both fibroblasts and iNLCs. In addition, both fibroblasts and iNLCs expressed *S100A4* and *VIM*. Expression of markers for neural stem cells only and neurons was present in iNLCs, but not fibroblasts. These results suggest that iNLCs are an intermediate cell type, expressing markers for both neural stem cells and neurons. Although iNLCs still express fibroblast markers, they differ from fibroblasts by expression of neuronal markers.

BIND imaging reveals metrics associated with iNLC growth

After 13–14 days of differentiation, we replated iNLCs on a BIND biosensor consisting of an array of individual biosensor wells in a standard 384-well plate reader format (Figure 2b). BIND biosensors consist of polymer surfaces embossed with grating structures of a precise and uniform periodicity and coated with titanium dioxide. When a broad wavelength source of light is projected to the biosensor surface, a particular resonance frequency is established, governed by the grating structure. The resulting monochromatic light is reflected off of the sensor surface to an imaging spectrophotometer and the PWV is captured and measured (Figure 2c). Increases in mass within ~150 nm of the sensor surface, including cultured cells which can be seeded and cultured on the biosensors, result in a directly proportional positive shift of the resonant reflected PWV. To facilitate neuronal cell growth and attachment, the biosensor was precoated with poly-ornithine and laminin, and titration of iNLC number indicated that an optimal cell density was 18 k cells cm^{-2}.

To image the iNLCs on the BIND biosensor, we utilized a BIND Scanner that measures PWV changes on a pixel-by-pixel basis at a spatial resolution of $3.75 \times 3.75\ \mu m^2$, enabling high-contrast visualization and subsequent segmentation of neuronal morphology. As seen from overlays of red fluorescent protein-expressing iNLCs, the BIND cell adhesion measurement captures neuronal morphology to a high degree (Figure 2d). The small footprint of the BIND Scanner allows it to be located within a tissue culture incubator, enabling high temporal resolution, time-lapse imaging of cellular responses at physiologic conditions (Figure 2e). As such, we used this imaging modality in a quantitative assay to measure changes in cellular morphology and attachment to the biosensor over the course of 24 h. Examples of sequential images of neurite outgrowth from plating of the cells on the BIND biosensor are shown in Figure 1a. We also observed that the neurite outgrowth tended to follow the linear grating structure of the BIND biosensor (Figure 2d). From these time-lapse images, we could monitor growth in terms of area and perimeter of the cells, as well as extract changes in PWV, a measure of the adhesion of the iNLCs to the biosensor.

To quantify the cellular phenotypes that could be observed on the BIND Scanner, we used BIND View software to segment the BIND scans and compute cell count, cell fraction (fractional area of the sensor covered by cells), cell perimeter and PWV normalized by local background. These metrics were averaged over each well for a given time point with time series over the first 5 h as shown in Figure 1b. The most dynamic region of cell growth and attachment to the surface occurred during the first hour after plating. This is qualitatively seen in the time-lapse videos (Supplementary Video 1) and time series plots of cell fraction, cell perimeter and PWV. As we were interested in identifying phenotypes associated with the temporal dynamics of neuronal growth and differentiation, we looked at baseline-normalized changes in the BIND metrics over the time course when cells have maximally attached. We refer to these as Δcell count, Δcell fraction, Δcell perimeter and ΔPWV (see Materials and Methods for more details). Boxplots summarizing the distribution of these Δmetrics as a function of patient grouping and Alda scale of lithium responsiveness are shown in Figure 1c.

Statistical analysis of BIND metrics

To model the associations between the BIND Δmetrics and subject groups, we used generalized linear models (GLMs)[18] with generalized estimating equations.[19] In addition, we included adjustments in these models for the following potential confounding experimental and clinical variables: the date each plate was imaged, sex and age. GLMs are similar to general linear models (for example, multiple regression, ANOVA) but allow greater flexibility in modeling outcome variables that are non-normally distributed using alternative distributions (for example, Poisson or negative binomial) and link functions (for example, log-transform or logit links). Mixed models using generalized estimating equation permit the appropriate handling of data that are hierarchically nested (that is, within subjects and plates) and thus likely to be correlated; modeling such correlations ensures appropriate estimation of standard errors and correct *P*-values in statistical tests. Further analyses controlled for cell count as a means of ensuring that observed phenotypes were not simply a proxy for cell death or segmentation error. Follow-up analyses utilized the same approach to examine the association between an ordinal measure of lithium-responsiveness, the Alda scale and any phenotypes associated with groups in the primary analysis.

Cellular measurements of iNLCs associated with patient lithium response

Figure 3a illustrates marginal means and 95% confidence intervals for each cellular metric, by subject group, drawn from GLM. There was a significant overall difference between patient groups for ΔPWV ($x^2 = 9.64$, $P = 0.008$) but not for Δcell count ($x^2 = 0.93$, $P = 0.63$), Δcell fraction ($x^2 = 2.26$, $P = 0.32$) or Δcell perimeter. After controlling for plate date, sex and age, the significant overall difference between patient groups persisted for ΔPWV ($x^2 = 7.02$, $P = 0.03$) but not for Δcell count ($x^2 = 2.88$, $P = 0.24$), Δcell fraction ($x^2 = 3.54$, $P = 0.17$) or Δcell perimeter ($x^2 = 2.45$, $P = 0.29$). For ΔPWV, Bonferroni-corrected *post hoc* pairwise tests indicated significant differences between BD lithium responsive and nonresponsive cells ($z = 2.65$, $P = 0.02$); neither group differed significantly from healthy controls ($z = -1.48$, $P = 0.42$ for controls ($n = 6$) versus BD lithium nonresponders ($n = 6$) and $z = 1.36$, $P = 0.51$ for controls versus BD Li responders ($n = 6$)).

Since Δcell count could be used as a measure of segmentation error and cell death, we incorporated this value into the GLM as an additional control. The ΔPWV result remained significant (Wald's test, $x^2 = 10.63$, $P = 0.005$), with Bonferroni-corrected *post hoc* pairwise differences observed between BD lithium responsive and nonresponsive ($z = 3.54$, $P = 0.001$) groups. The remaining two phenotypes Δcell fraction ($x^2 = 3.40$, $P = 0.18$) and Δcell perimeter ($x^2 = 1.00$, $P = 0.61$) remained nonsignificant. The estimated marginal means derived from the GLM for Δcell fraction, Δcell perimeter and ΔPWV, corrected for patient age and sex, plate date and Δcell count, are shown in Figure 3b with 95% confidence intervals.

We also examined the effects of lithium exposure in the patients, as this could contribute to the differences in observed iNLC ΔPWV. In all, five of six lithium responders, and five of six

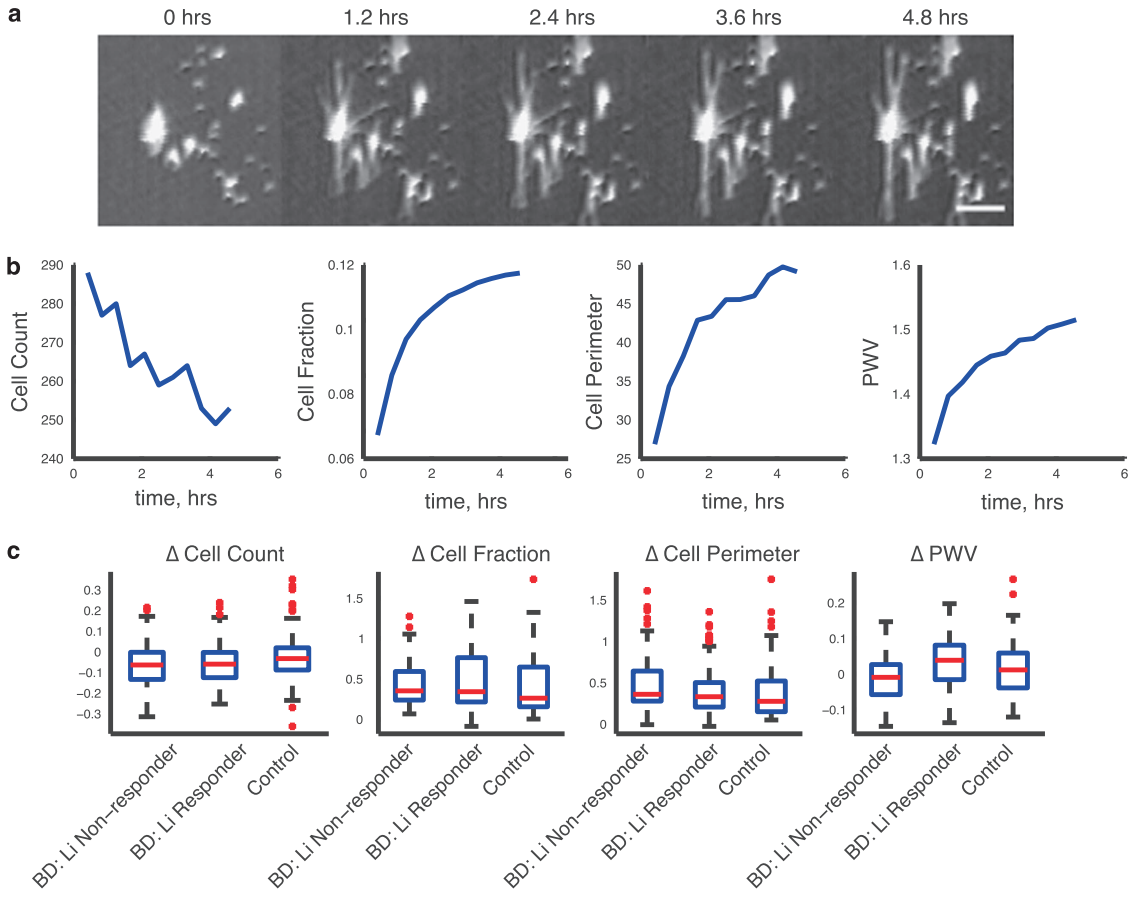

Figure 1. BIND imaging phenotypes of human iNLCs. (**a**) BIND images of a representative field (scale bar, 100 μm) at 1.2-h intervals beginning at plating of the cells. Imaging resolution is sufficient to capture outgrowth of cellular processes. (**b**) Time series quantification of BIND metrics—cell count, cell fraction, perimeter and PWV—over the first 4 h of continuous imaging shows that the most dynamic region of cellular attachment and growth occurs in the first 1.5 h. (**c**) Distribution of baseline-normalized changes in BIND metrics for each phenotype, by patient group. BD, bipolar disorder; iNLC, induced neuronal-like cell; PWV, peak wavelength value.

lithium nonresponders, were treated with lithium at the time of study enrollment, so lithium exposure in the patients themselves is unlikely to account for observed differences in iNLC ΔPWV phenotypes. In GLM models, lithium exposure was not associated with differential ΔPWV ($\beta\Delta_{PWV} = 0.0009$; SE = 0.018, $P = 0.96$); whereas patient group differences remained significant ($x^2 = 70.2$, $P = 0.03$) in *post hoc* pairwise comparison of responders and nonresponders ($z = 2.64$, $P = 0.03$).

Ordinal measurements of lithium response

In follow-up analysis, we examined association between ΔPWV and an ordinal measure of lithium response, the Alda scale, rather than dichotomizing the measure of lithium responsivity. As anticipated, these models also showed significant association ($\beta\Delta_{PWV} = 0.008$; SE = 0.003, $P = 0.008$), which persisted with inclusion of Δcell count ($\beta\Delta_{PWV} = 0.009$; SE = 0.003, $P = 0.002$; Figure 3c). Taken together, these findings support the notion that there are cellular correlates of lithium response in patients that can be readily monitored and observed *in vitro* using label-free optical imaging methodology.

Absence of cellular phenotypes in fibroblasts

Although the primary analyses focused on characterization of transdifferentiated cells, it is possible that the phenotypes observed are also present in the cultured fibroblasts. To address this question, we performed the same BIND measurements and GLM analyses on a subset of the patient fibroblasts ($n = 4$ healthy controls, $n = 4$ BD lithium responders, $n = 4$ BD lithium nonresponders). Using a GLM correcting for plate date, sex and age, we did not observe statistically significant differences in the marginal means for ΔPWV by groups, including *post hoc* contrasts between BD lithium responsive and non-responsive groups ($x^2 = 0.61$, $P = 0.74$). Likewise, correcting for Δcell count did not produce significant differences ($x^2 = 0.62$, $P = 0.73$).

Effects of acute lithium treatment

We also investigated the effect of acute lithium exposure on the BIND phenotypes, by examining lithium at three concentrations (0.3 mM, 0.8 mM, 1 mM) added to the cells at the time of plating on the biosensor. Once again, GLM models were used to examine dose effect, correcting for plate date, sex and age. Supplementary Figure 2 illustrates the PWV measurement by lithium dose (x axis) and experimental group (color). No significant main effects of treatment were identified ($\beta\Delta_{PWV} = 0.006$; SE = 0.005; $P = 0.24$), nor any evidence of a group-by-treatment interaction ($x^2 = 4.66$, $P = 0.59$).

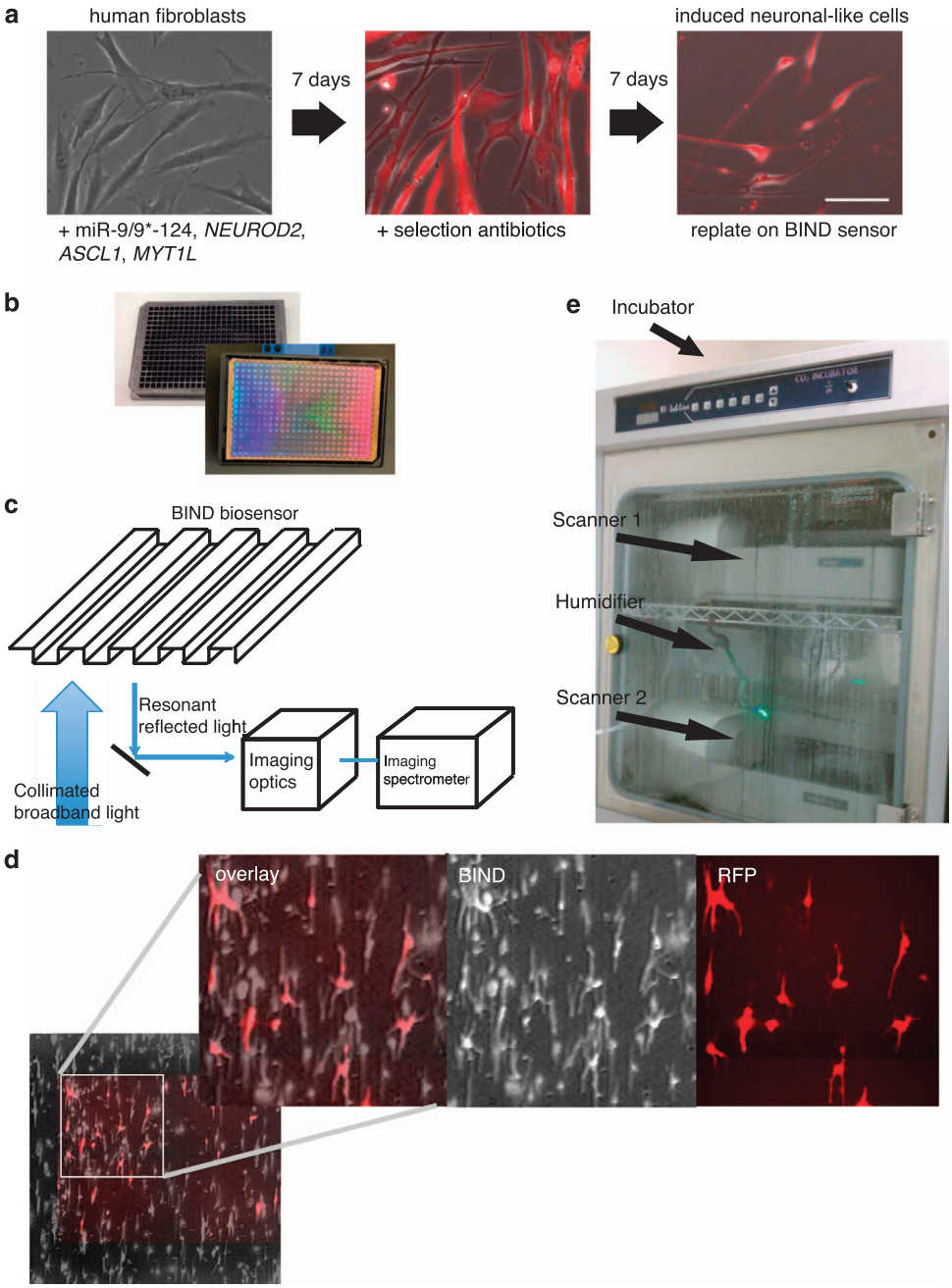

Figure 2. Generation of BD patient-derived iNLCs and BIND imaging. (**a**) Fibroblasts transduced with miR-9/9*-124, *NEUROD2*, *ASCL1* and *MYT1L* undergo selection 3 days after lentiviral infection. RFP expression indicates miR-9/9*-124 expression. Morphological changes occur while cells are undergoing selection. At 14 days posttransduction, cells have elongated processes resembling neurite outgrowth. (**b**) Nanostructured photonic crystal biosensors form the bottom surface of a 384-well plate onto which cells can adhere. Collimated broadband light is projected onto the biosensor, and the resulting resonant reflected light is collected and recorded by an imaging spectrometer, illustrated in **c**. (**d**) An overlay of the RFP indicator and BIND scan show that detailed morphology of cells can be captured by the BIND scan and is similar to the morphology seen by fluorescent light microscopy of the RFP indicator. (**e**) Incubated BIND Scanner allows long-term time-lapse imaging of iNLCs. BD, bipolar disorder; iNLC, induced neuronal-like cell; RFP, red fluorescent protein.

DISCUSSION

In this investigation of 18 patient-derived induced neuron lines, we identified a cellular phenotype associated with the lithium responsiveness of bipolar 1 disorder patients. The phenotype itself, ΔPWV, can be interpreted as a measure of adhesion of cells to the biosensor.[13] BD lithium nonresponder cells adhered less strongly than cells from bipolar patients who respond well to lithium. Interestingly, cells from control individuals without BD appeared to be intermediate between lithium-responsive and nonresponsive BD patient cells. Importantly, no significant phenotypic differences were observed for this measure in cultured fibroblasts, supporting the potential utility of using transdifferentiated cells.

The quantitative metric used in this study, ΔPWV, represents the change in wavelength of light reflected from an optical biosensor surface. This change in resonant reflected light is mediated by

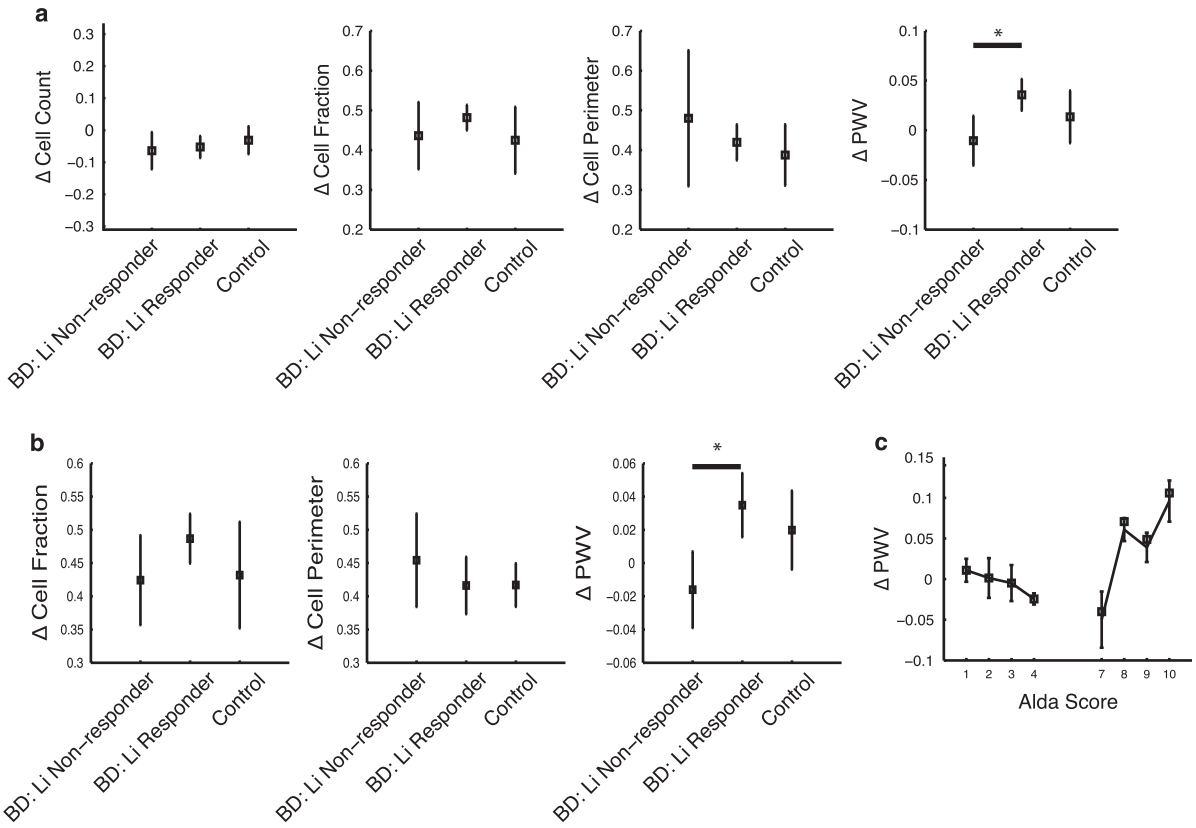

Figure 3. Correlation of cellular BIND metrics to clinical features. (**a**) The four plots illustrate marginal means and 95% confidence intervals for the four cellular phenotypes identified using the BIND Scanner, with adjustment for age, sex and experiment. The asterisk denotes a significant difference in ΔPWV between BD Li Non-responders and BD Li Responders as indicated by Bonferroni corrected *post hoc* pairwise testing ($P = 0.02$). (**b**) Marginal means and 95% confidence intervals for change in cell fraction, cell perimeter and PWV, with adjustment for change in cell count. (**c**) Results for change in PWV, adjusted as in **b**, by Alda score (degree of improvement with lithium) group. BD, bipolar disorder; PWV, peak wavelength value.

increases in mass detected within the evanescent field that extends approximately 200 nm from the sensor surface. Many different cell types can adhere to optical biosensors coated with extracellular matrix components that bind to specific integrins expressed on the cell surface. The role of integrin–extracellular matrix interactions on optical biosensors contributing to ΔPWV measurements has been established in cell lines endogenously expressing specific integrins. For example, the human 8866 B cell line endogenously expresses the α4β7 integrin, which is known to be a ligand for the extracellular matrix protein, MadCAM.[13] The addition of 8866 cells to MadCAM-coated biosensors elicits a strong ΔPWV response whereas a minimal response is measured when biosensors are coated with a control protein. Furthermore, the ΔPWV response of 8866 cells on MadCAM-coated sensors is blocked to completion by an α4-specific antibody, demonstrating that the ΔPWV signal is mediated by integrin–CAM interactions. Similarly, Jurkat cells expressing the α4β1 integrin produce a ΔPWV signal on optical biosensors coated with VCAM (unpublished results). Specific inhibitors of the α4β1-VCAM interaction completely inhibit this signal, as does the addition of EDTA to chelate divalent cations known to be required for integrin-mediated cell adhesion. Taken together, these results demonstrate that the ΔPWV signal is a cell adhesion-mediated measurement governed by integrin–CAM interactions. The positive shift in the reflected wavelength upon integrin–CAM engagement can be explained by an increase in cellular mass entering the evanescent field as the cell adheres more strongly to the sensor surface.

Strengths of the present study include a single, clinically-homogeneous and rigorously phenotyped cohort, including matched psychiatrically screened healthy controls. Treatment response was assessed using a validated, gold-standard measure of lithium responsiveness.[16] Conversely, a key caveat is the modest effect size observed, and the substantial risk of type 1 error arising in this relatively small cohort. Despite evidence that lithium response is familial,[15,20,21] the stability of such response within an individual over time remains to be established. Furthermore, extrapolating from our cellular observations to mature neurons is difficult; and although we have shown that the transformed fibroblasts express structural neuronal markers, they still comprise a heterogeneous population of cells which require additional differentiation before they are able to fire action potentials or form synapses or synapse-like structures.[9] Nonetheless, the potential utility of a cell-based model of lithium response in BD should be apparent, and more generally, a biomarker for lithium response could have substantial clinical value, allowing more precise weighing of risks and benefits of lithium treatment. As one of only two pharmacotherapies in all of psychiatry was shown to diminish suicide risk,[22] lithium treatment remains a viable but underused clinical option where the availability of a biomarker could increase patient and clinician acceptability.

We did not observe an acute effect of lithium exposure in these assays. *In vitro* investigation of lithium remains challenging because of an apparently narrow therapeutic window (that is, toxicity at higher doses) as well as a lack of clear correspondence between *in vitro* and *in vivo* lithium levels. We note that, in human studies in bipolar disorder, lithium may require 6–8 weeks or more for clinical efficacy, so it is possible that chronic lithium exposure

would yield more relevant results. We also did not observe a significant reduction in cell growth among BD patient cells compared with healthy controls, which might have been anticipated based on structural brain imaging showing a decrease in gray matter volume in the brains of BD patients versus controls.[23] However, such decreases have been attributed to oxidative stress-induced apoptosis,[24] something which our cellular model may not capture.

The cell adhesion phenotype we observed is consistent with other emerging observations in psychiatric disease models. Cells derived from schizophrenia patients have been associated with less adhesion and increased motility,[25] and multiple postmortem brain studies of psychiatric disease patients show alterations in the polysialylated neural cell adhesion molecule,[26,27] a protein that has a key role in cell migration. In addition, genome-wide association studies of schizophrenia and BD implicate genes involved in cell adhesion.[28,29]

The potential mechanisms by which variation in cell adhesion could give rise to a connectopathy lies in considering the role that cell adhesion molecules have in affecting synaptic dynamics and structural plasticity in neurons. Pathology in the microstructure of synapses is associated with psychiatric disorders,[30] and the regulation of synaptic plasticity depends, in large part, on appropriate functioning of the actin cytoskeleton to support vesicle cycling and postsynaptic receptors.[31] Recent findings in a rodent model have correlated a behavioral phenotype with a cytoskeletal defect: in particular, a duplication of *SHANK3*, a synaptic scaffold and actin-binding protein, was associated with manic-like behavior similar to the hyperkinetic phenotype of patients with *SHANK3* duplications. Increases in F-actin levels, mediated through dysregulation of *ARP2/3* complexes, which are central regulators of actin-mediated remodeling and cell motility, were observed in hippocampal neurons cultured from these mice.[32] Other lines of evidence have demonstrated that cadherins and catenins engage in activity-dependent modulation of axon–spine contacts.[33] Given that lithium has been demonstrated to affect neuron growth cones[34] and regulate cytoskeletal dynamics via *GSK3*β inhibition,[35] it is suggested that our observed cell adhesion phenotype may provide an initial step in characterizing the pathophysiology of BD and efficiently screening for novel therapeutics.

A key advantage of the cellular approach we describe is that it allows rapid characterization of many cellular phenotypes with a scalable, label-free platform, making it amenable to high-throughput chemical screens, RNAi-based screens, large-scale investigations of genome editing, and potentially, development of clinical diagnostic tools. The extent of its utility will be clarified by measurement of phenotypes across disorders and treatments; at minimum, it should facilitate efforts to elucidate mechanism of action of the gold-standard treatment for a disorder that contributes substantially to morbidity from psychiatric disease worldwide.

CONFLICT OF INTEREST

RHP has received consulting fees or served on scientific advisory boards for Proteus Biomedical, Pamlab, PerfectHealth, Pfizer, PsyBrain, Genomind and RIDventures, research grant support from Proteus Biomedical and royalties from UBC. The remaining authors declare no conflict of interest.

ACKNOWLEDGMENTS

We acknowledge the helpful discussion and feedback from members of the Perlis, Haggarty and Crabtree Laboratories and X-Body Biosciences. We also acknowledge Bob Weinberg and Didier Trono for the use of lentiviral packaging plasmids deposited with Addgene. This work was supported through funding from the National Institute of Mental Health (R21MH093958, R33MH087896). Biobank collection was further supported by the Stanley Center for Psychiatric Research.

REFERENCES

1 Osby U, Brandt L, Correia N, Ekbom A, Sparen P. Excess mortality in bipolar and unipolar disorder in Sweden. *Arch Gen Psychiatry* 2001; **58**: 844–850.
2 Vos T, Flaxman AD, Naghavi M, Lozano R, Michaud C, Ezzati M *et al.* Years lived with disability (YLDs) for 1160 sequelae of 289 diseases and injuries 1990-2010: a systematic analysis for the Global Burden of Disease Study 2010. *Lancet* 2012; **380**: 2163–2196.
3 Yatham LN, Kennedy SH, Parikh SV, Schaffer A, Beaulieu S, Alda M *et al.* Canadian Network for Mood and Anxiety Treatments (CANMAT) and International Society for Bipolar Disorders (ISBD) collaborative update of CANMAT guidelines for the management of patients with bipolar disorder: update 2013. *Bipolar disord* 2013; **15**: 1–44.
4 Geddes JR, Goodwin GM, Rendell J, Azorin JM, Cipriani A, Ostacher MJ *et al.* Lithium plus valproate combination therapy versus monotherapy for relapse prevention in bipolar I disorder (BALANCE): a randomised open-label trial. *Lancet* 2010; **375**: 385–395.
5 Chambers SM, Fasano CA, Papapetrou EP, Tomishima M, Sadelain M, Studer L. Highly efficient neural conversion of human ES and iPS cells by dual inhibition of SMAD signaling. *Nat Biotechnol* 2009; **27**: 275–280.
6 Shi Y, Kirwan P, Smith J, Robinson HPC, Livesey FJ. Human cerebral cortex development from pluripotent stem cells to functional excitatory synapses. *Nat Neurosci* 2012; **15**: 477–486.
7 Wang Y, Dolmetsch R. In vitro human corticogenesis. *Neuron* 2013; **77**: 379–381.
8 Vierbuchen T, Ostermeier A, Pang ZP, Kokubu Y, Südhof TC, Wernig M. Direct conversion of fibroblasts to functional neurons by defined factors. *Nature* 2010; **463**: 1035–1041.
9 Yoo AS, Sun AX, Li L, Shcheglovitov A, Portmann T, Li Y *et al.* MicroRNA-mediated conversion of human fibroblasts to neurons. *Nature* 2011; 228–231.
10 Ladewig J, Mertens J, Kesavan J, Doerr J, Poppe D, Glaue F *et al.* Small molecules enable highly efficient neuronal conversion of human fibroblasts. *Nat Methods* 2012; **9**: 575–578.
11 Qiang L, Fujita R, Abeliovich A. Remodeling neurodegeneration: somatic cell reprogramming-based models of adult neurological disorders. *Neuron* 2013; **78**: 957–969.
12 Faull RJ, Ginsberg MH. Inside-out signaling through integrins. *J Am Soc Nephrol* 1996; **7**: 1091–1097.
13 Bova MP, Nguyen L, Wallace W, Garrido C, Xu Y-Z, Semko C *et al.* A label-free approach to identify inhibitors of alpha4beta7-mediated cell adhesion to MadCAM. *J Biomol Screen* 2011; **16**: 536–544.
14 Shamah SM, Cunningham BT. Label-free cell-based assays using photonic crystal optical biosensors. *Analyst* 2011; **136**: 1090–1102.
15 Grof P, Duffy A, Cavazzoni P, Grof E, Garnham J, MacDougall M *et al.* Is response to prophylactic lithium a familial trait? *J Clin Psychiatry* 2002; **63**: 942–947.
16 Manchia M, Adli M, Akula N, Ardau R, Aubry JM, Backlund L *et al.* Assessment of response to lithium maintenance treatment in bipolar disorder: a Consortium on Lithium Genetics (ConLiGen) Report. *PLoS One* 2013; **8**: e65636.
17 Stewart SA, Dykxhoorn DM, Palliser D, Mizuno H, Yu EY, An DS *et al.* Lentivirus-delivered stable gene silencing by RNAi in primary cells. *RNA* 2003; **9**: 493–501.
18 Cohen J, Cohen P, West SG, Aiken LS. *Applied Multiple Regression/Correlation Analysis for the Behavioral Sciences*, 3rd edn. Lawrence Erlbaum Associates: Mahwah, NJ, USA, 2002.
19 Self SG, Liang KY. Asymptotic properties of maximum likelihood estimators and likelihood ratio tests under nonstandard conditions. *J Am Stat Asso* 1987; **82**: 398.
20 Duffy A, Alda M, Kutcher S, Cavazzoni P, Robertson C, Grof E *et al.* A prospective study of the offspring of bipolar parents responsive and nonresponsive to lithium treatment. *J Clin Psychiatry* 2002; **63**: 1171–1178.
21 Grof P, Duffy A, Alda M, Hajek T. Lithium response across generations. *Acta Psychiatr Scand* 2009; **120**: 378–385.
22 Cipriani A, Hawton K, Stockton S, Geddes JR. Lithium in the prevention of suicide in mood disorders: updated systematic review and meta-analysis. *BMJ* 2013; **346**: f3646.
23 Bora E, Fornito A, Yücel M, Pantelis C. Voxelwise meta-analysis of gray matter abnormalities in bipolar disorder. *Biol Psychiatry* 2010; **67**: 1097–1105.
24 Berk M, Kapczinski F, Andreazza AC, Dean OM, Giorlando F, Maes M *et al.* Pathways underlying neuroprogression in bipolar disorder: focus on inflammation, oxidative stress and neurotrophic factors. *Neurosci Biobehav Rev* 2011; **35**: 804–817.
25 Fan Y, Abrahamsen G, Mills R, Calderón CC, Tee JY, Leyton L *et al.* Focal adhesion dynamics are altered in schizophrenia. *Biol Psychiatry* 2013; **74**: 418–426.
26 Nacher J, Guirado R, Castillo-Gómez E. Structural plasticity of interneurons in the adult brain: role of PSA-NCAM and implications for psychiatric disorders. *Neurochem Res* 2013; **38**: 1122–1133.
27 Varea E, Guirado R, Gilabert-Juan J, Martí U, Castillo-Gómez E, Blasco-Ibáñez JM *et al.* Expression of PSA-NCAM and synaptic proteins in the amygdala of psychiatric disorder patients. *J Psychiatr Res* 2012; **46**: 189–197.

28 Sprooten E, Fleming KM, Thomson PA, Bastin ME, Whalley HC, Hall J *et al.* White matter integrity as an intermediate phenotype: exploratory genome-wide association analysis in individuals at high risk of bipolar disorder. *Psychiatry Res* 2013; **206**: 223–231.
29 Hill MJ, Jeffries AR, Dobson RJ, Price J, Bray NJ. Knockdown of the psychosis susceptibility gene ZNF804A alters expression of genes involved in cell adhesion. *Hum Mol Genet* 2012; **21**: 1018–1024.
30 Blanpied TA, Ehlers MD. Microanatomy of dendritic spines: emerging principles of synaptic pathology in psychiatric and neurological disease. *Biol Psychiatry* 2004; **55**: 1121–1127.
31 Cingolani LA, Goda Y. Actin in action: the interplay between the actin cytoskeleton and synaptic efficacy. *Nat Rev Neurosci* 2008; **9**: 344–356.
32 Han K, Holder JL Jr, Schaaf CP, Lu H, Chen H, Kang H *et al.* SHANK3 overexpression causes manic-like behaviour with unique pharmacogenetic properties. *Nature* 2013; **503**: 72–77.
33 Takeichi M, Abe K. Synaptic contact dynamics controlled by cadherin and catenins. *Trends Cell Biol* 2005; **15**: 216–221.
34 Williams RSB, Cheng L, Mudge AW, Harwood AJ. A common mechanism of action for three mood-stabilizing drugs. *Nature* 2002; **417**: 292–295.
35 Grimes CA, Jope RS. The multifaceted roles of glycogen synthase kinase 3b in cellular signaling. *Prog Neurobiol* 2001; **65**: 391–426.

Supplementary Information accompanies the paper on the Translational Psychiatry website (http://www.nature.com/tp)